



UNIVERSITY OF LEEDS

This is a repository copy of *Non-linear soil behaviour on high speed rail lines*.

White Rose Research Online URL for this paper:

<http://eprints.whiterose.ac.uk/146304/>

Version: Accepted Version

Article:

Dong, K, Connolly, DP, Laghrouche, O et al. (2 more authors) (2019) Non-linear soil behaviour on high speed rail lines. *Computers and Geotechnics*, 112. pp. 302-318. ISSN 0266-352X

<https://doi.org/10.1016/j.compgeo.2019.03.028>

© 2019 Elsevier Ltd. All rights reserved. Licensed under the Creative Commons Attribution-Non Commercial No Derivatives 4.0 International License (<https://creativecommons.org/licenses/by-nc-nd/4.0/>).

Reuse

This article is distributed under the terms of the Creative Commons Attribution-NonCommercial-NoDerivs (CC BY-NC-ND) licence. This licence only allows you to download this work and share it with others as long as you credit the authors, but you can't change the article in any way or use it commercially. More information and the full terms of the licence here: <https://creativecommons.org/licenses/>

Takedown

If you consider content in White Rose Research Online to be in breach of UK law, please notify us by emailing eprints@whiterose.ac.uk including the URL of the record and the reason for the withdrawal request.



eprints@whiterose.ac.uk
<https://eprints.whiterose.ac.uk/>

Non-linear Soil Behaviour on High Speed Rail Lines –An equivalent linear approach

Authors:

K. Dong, D.P. Connolly, O. Laghrouche, P.K. Woodward, P. Alves Costa

Abstract (200 words)

This paper gives new insights into non-linear subgrade behaviour on high speed railway track dynamics. First, a novel semi-analytical model is developed which allows for soil stiffness and damping to dynamically change as a function of strain. The model uses analytical expressions for the railroad track, coupled to a thin-layer element formulation for the ground. Material non-linearity is accounted for using a 'linear equivalent' approach which iteratively updates the soil material properties. It is validated using published datasets and in-situ field data. Four case studies are used to investigate non-linear behaviour, each with contrasting subgrade characteristics. Considering an 18 tonne axle load, the critical velocity is significantly lower than the linear case, and rail deflections are up to 30% higher. Furthermore, at speeds close-to, but below the non-linear critical velocity, dynamic amplification is highly sensitive to small increases in train speed. These findings are dependent upon soil material properties, and are important for railway track-earthwork designers because often 70% of the linear critical velocity is used as a design limit. This work shows that designs close to this limit may be still at risk of high dynamic effects, particularly if line speed is increased in the future.

Keywords (6): Soil-subgrade non-linearity; railroad track stiffness; railway critical velocity; Rail-track dynamic amplification; Thin-layer element method (TLM), high speed rail track design

1. Introduction

Increases to operational train speed mean that it is more likely vehicles will induce dynamic effects within the supporting track and soil structure. This is because as train speed increases towards the elastic wave speeds in the track-ground system, dynamic wave propagation increases. The speed of maximum dynamic amplification is known as the 'critical velocity' ([1], [2]) and in certain cases has been measured to be as low as 65 m/s ([2], [3]). This is significantly below the operational speed of typical high speed lines/trains (85m/s), and if large track displacements are induced, the track will degrade quickly and hence require frequent maintenance.

To investigate this problem, early researchers proposed the use of analytical approaches for the track and soil response in the frequency domain ([1], [4], [5], [6]). These were expanded upon by using integral transform methods for the simulation of more complex systems like layered ground. This allowed for more complex and layered soil

profiles to be investigated ([2], [3], [7], [8], [9]). Alternatively, semi-analytical formulations were proposed (e.g. thin-layer element method [10]), which allowed for even greater flexibility in soil profiles to be investigated ([11], [12], [13]).

Rather than model the track using analytical expressions, ‘two-and-a-half’ dimensional models (2.5D) for both the track and soil were also proposed ([14], [15], [16], [17], [18], [19]). These assume the track is invariant in the direction of train passage thus only requiring the problem to be discretised into 2D, before recovering the 3D response using a transform. This is advantageous because it allows for the modelling of relatively complex track and soil geometry, with much lower run times compared to 3D models.

The 2.5D approach is useful for simulation of concrete slab track systems because the geometry doesn’t vary greatly in the direction of train passage. However, ballasted tracks have discretely spaced sleepers which cannot be simulated using this technique. Therefore ([20], [21], [22], [23]) proposed periodic models where each repetitive sleeper bay was classified as a cell. The periodic modes of the slice are computed and then a Floquet transform used to convert the response of the single slice into an infinitely long domain.

Periodic modelling is useful when track geometry is repetitive, however it is challenging to use when this is not the case (e.g. transition zones or singular defects). In these cases, 3D models are required. A variety of these have been proposed in the frequency domain, typically using finite elements for the track and boundary elements to prevent reflections from outgoing waves ([24], [25], [26], [27], [28]). Alternatively, time domain formulations have been proposed which can permit more complex material models, however present more challenges related to boundary reflections ([29], [30], [31], [32], [33], [34], [35], [36], [37]).

A challenge with the majority of analytical and numerical approaches proposed for railway modelling is the assumption of linear elastic material behaviour. However, when the train speed is high, large strains are often induced in the soil, thus causing non-linear stiffness and damping behaviour ([3], [38], [15]). This results in quite different track behaviour (i.e. deflection) compared to the case in which non-linearity is not accounted for.

To include non-linear material effects, [2], [3], [7] and [29] used models with manually adjusted soil stiffness to predict the response of track in Ledsgard, Sweden. Furthermore, [39] used a similar approach to investigate the response of a piled embankment. A challenge with this approach is that manually choosing stiffness’ values is often inaccurate and it is only practical to implement stiffness changes over large depths of soil (e.g. across an entire soil layer). Alternatively, [40] considered non-linear elastic behaviour when modelling the response of the same Swedish site using a time domain 3D finite element model. This allowed for the non-linearity of all finite elements to be considered individually, however a challenge with constitutive models though is that they require a large number of input parameters, many of which are difficult to quantify. Therefore, [15] proposed a 2.5D finite/infinite element method, coupled with an iterative, ‘linear equivalent’ procedure that used strain levels and degradation curve data to

automatically adjust material stiffness and damping based upon strain levels. Again, an ‘element-by-element’ non-linear approach was used and strong agreement was achieved compared to the Swedish data.

To compare the difference between a constitutive non-linear material model and a linear equivalent model, [38] compared both using a 3D finite element approach. To reduce the complexity of the linear equivalent formulation, a horizontal ‘layer-by-layer’ ‘linear equivalent’ approach was used. This assumed that the same non-linear changes to material properties below the track centre-line also propagated to the far-field. Therefore the elastic material properties away from the track were considered to degrade in an overly conservative manner. Despite this assumption, for locations near the track, it was found that the linear equivalent approach gave similar results but with reduced computational requirements.

This paper therefore builds upon this linear equivalent approach to simulate soil non-linearity. First, a frequency domain model is described, where the track is modelled analytically and the soil modelled semi-discretely using the thin-layer element method. The track-ground models are coupled and the overall model is computed in an iterative (thin) ‘layer-by-layer’ manner to include the effects of non-linearity. This greatly reduces the computational time, and due to the very thin nature of elements used in the thin-layer method, stiffness changes due to non-linearity can be simulated with much finer granularity compared to [38].

2. Model description

The track-ground system is modelled using a sub-structuring approach [12]. An analytical model is used to calculate the track response, while the thin-layer element method is used to compute the soil response. They are then coupled taking into account the compatibility of displacements and equilibrium of loads in the vertical direction (thus implying relaxed boundary conditions [41]). Non-linearity is adopted in the soil response using an ‘equivalent linear’ methodology. Although the model is by definition ‘linear equivalent’, the term ‘non-linear’ is also used interchangeably to denote the same meaning.

2.1 Track model

The track is modelled in the wavenumber-frequency domain as described in the works of [13], [42], [9], and [12]. Ballasted track (Figure 1) and slab track (Figure 2) are described using different formulations, however for brevity, only the ballasted track is described here. The governing equations for the ballasted track are shown in Equation 1, where E_b is the ballast Young’s modulus; h_b is the ballast thickness; C_p is the ballast compressional wave speed, and \tilde{u}_r , \tilde{u}_s and \tilde{u}_{bb} are the rail, sleeper, and ballast (bottom) displacements respectively, with the tilde ‘~’ denoting the frequency domain.

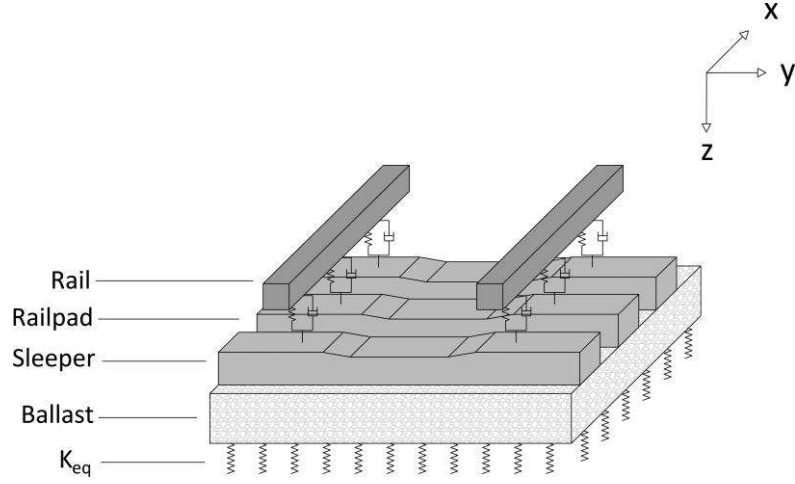


Figure 1: Ballasted track structure

Furthermore, k_p^* is the complex stiffness of the railpad, which is defined as, $k_p^* = k_p(1 + i\omega c_p)$. In this formula, k_p is the railpad stiffness, c_p is the viscous damping, $i = \sqrt{-1}$ and ω is the frequency. Finally, k_x is the Fourier image of x (direction of train passage), m_r and m_s are the mass of rail per metre and the distributed mass of sleepers/ties respectively, $2b$ is the track width, and P is the downward vertical force applied at the railhead.

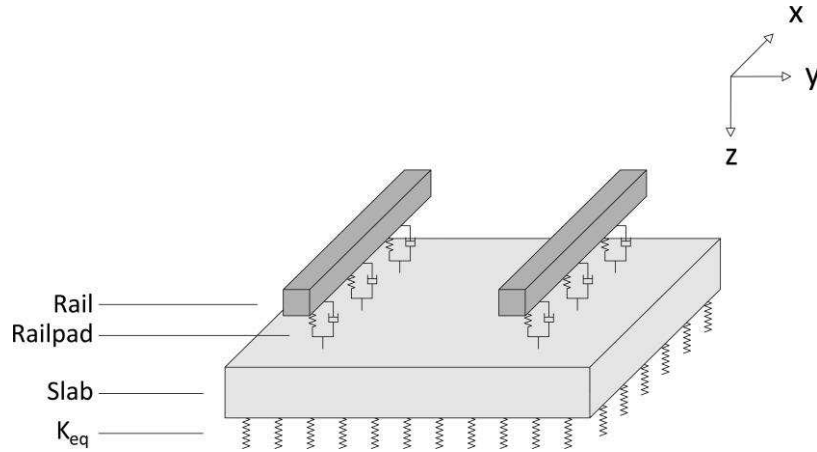


Figure 2: Slab track structure

$$\begin{bmatrix} EI_r k_x^4 + k_p^* - \omega^2 m_r & -k_p^* & 0 \\ -k_p^* & k_p^* + \frac{2\omega E_b^* b \alpha}{\tan\left(\frac{\omega h_b}{C_p}\right) C_p} - \omega^2 m_s & \frac{-2\omega E_b^* b \alpha}{\sin\left(\frac{\omega h_b}{C_p}\right) C_p} \\ 0 & \frac{-2\omega E_b^* b \alpha}{\sin\left(\frac{\omega h_b}{C_p}\right) C_p} & \frac{2\omega E_b^* b \alpha}{\tan\left(\frac{\omega h_b}{C_p}\right) C_p} + k_{eq} \end{bmatrix} \begin{Bmatrix} \tilde{u}_r(k_x, \omega) \\ \tilde{u}_s(k_x, \omega) \\ \tilde{u}_{bb}(k_x, \omega) \end{Bmatrix} = \begin{Bmatrix} \tilde{P}(k_x, \omega) \\ 0 \\ 0 \end{Bmatrix} \quad (1)$$

Coupling between the analytical track model and the soil is implemented using an equivalent complex stiffness (k_{eq}) in the vertical direction only, computed using the thin-

layer method, and defined by Equation 2. As train speed increases, wave energy propagates to greater depths in the soil, meaning the deeper soil layers affect the track response. Therefore, the accurate coupling across this interface becomes increasingly important as the train speed approaches the critical velocity.

$$\tilde{k}_{eq}(k_x, \omega) = \frac{2\pi}{\int_{-\infty}^{+\infty} \tilde{u}_{zz}^G(k_x, k_y, 0, \omega) C_{tg} dk_y} \quad (2)$$

In Equation 2, \tilde{u}_{zz}^G is the Green's function of vertical displacement of the uppermost soil surface ($z=0$) and corresponds to the z -direction term (Q33) of the stationary dynamic flexibility matrix Q in the transformed domain [13]. k_y is the Fourier image of y (lateral direction). C_{tg} is a factor used to adjust the coupling depending upon whether the track is slab or ballasted. In the case of a ballasted track, displacements at the track centre are used for computation (Equation 3), as demonstrated in Figure 3. For the slab track, the mean displacement across the interface boundary is used (Equation 4) [9][13], via the approach outlined in Figure 4. For both track cases, relaxed boundary conditions are assumed (i.e. coupling is only accounted for in the vertical direction).

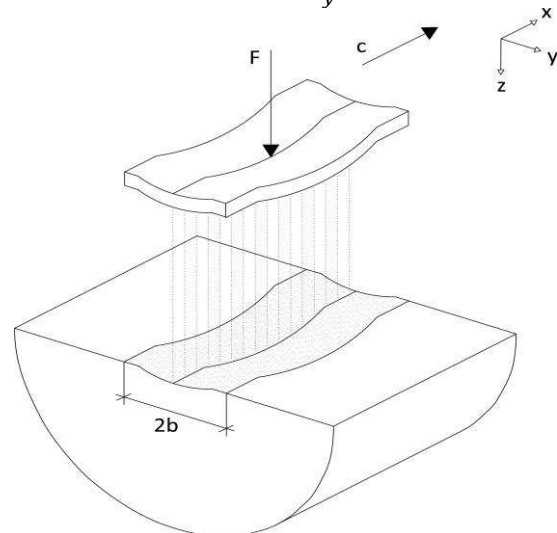
$$C_{tg} = \frac{\sin(k_y b)}{k_y b} \quad (3)$$


Figure 3: Illustration of scaling factor of the track-ground coupling for ballasted track

$$C_{tg} = \frac{\sin(k_y b)^2}{(k_y b)^2} \quad (4)$$

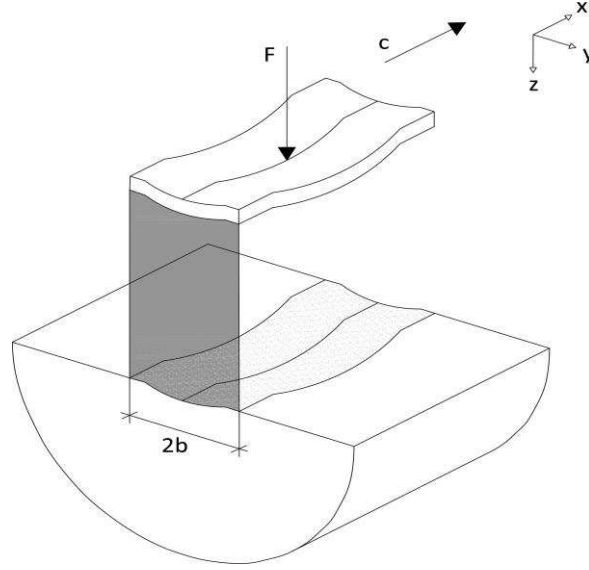


Figure 4: Illustration of scaling factor of the track-ground coupling for slab track

2.2 Soil model

The stresses, strains and displacements within the 3D soil stratum are computed using the thin-layer method. To do so, the domain is discretised into a series of thin horizontal layers. Three nodes are used for each element (thin-layer) and the analytical wave equation is used to compute the response in both horizontal directions. The problem is solved in the frequency-wavenumber domain, using eight thin-layers per wavelength to ensure accuracy [12].

2.2.1 Equivalent stiffness formulation

Solving the system of equations (Equation 1 and Equation 2) returns the displacements of all track components, including the lowermost layer (u_{bb}), due to a vertical unit load on the rail ([9] [12]). These displacements can then be scaled linearly to account for a point load of arbitrary magnitude. However, to compute soil displacements for a load of arbitrary magnitude, the displacement Green's function $R_u(k_x, k_y, \omega)$ for each individual soil thin layer is scaled as:

$$R_u(k_x, k_y, \omega) = (L(k_x, \omega)C_{tg})u^g(k_x, k_y, \omega) \quad (5)$$

Where $u^g(k_x, k_y, \omega)$ is the ground displacement Green's function in the wavenumber-frequency domain. Similarly, $u^g(k_x, k_y, \omega)$ can be replaced by the stress and strain Green's functions: $\sigma^g(k_x, k_y, \omega)$ and $\varepsilon^g(k_x, k_y, \omega)$, to obtain the stress/strain response in the soil. The strain Green's function is required to compute the soil strain levels needed for the equivalent linear formulation. Also, $L(k_x, \omega)C_{tg}$ is the load scale function, where C_{tg} is given in Equation 3 and Equation 4. $L(k_x, \omega)$ represents the load transmitted by the track to the ground and is computed by multiplication of the equivalent stiffness and lower track displacement:

$$L(k_x, \omega) = k_{eq}(k_x, \omega) \times u_{bb}(k_x, \omega) \quad (6)$$

Finally, the ground response (displacement, stress or strain) for an individual layer (e.g. soil surface as shown in Figure 24) in the time-time-space domain is computed by inverting the scaled Green's function using the inverse Fourier transform:

$$R(x, y, t) = \frac{1}{(2\pi)^3} \int_{-\infty}^{\infty} \int_{-\infty}^{\infty} \int_{-\infty}^{\infty} R(k_x, k_y, \omega) e^{i(\omega t - k_x x - k_y y)} dk_x dk_y d\omega \quad (7)$$

It is worth noting that because the TLM model is computed in the wavenumber-frequency domain, the moving load effect is taken into account using the shift property of the Fourier transform that allows frequency to be related to wavenumber, i.e., $\omega = \Omega - k_x c$, where Ω is the excitation frequency (set to 0Hz in this work), k_x is the wavenumber in the direction of moving load, and c is the moving load velocity.

2.2.2 Equivalent linear formulation

When the soil is subject to small strains, the stresses and strains are directly proportional, meaning the soil response can be considered linear and elastic (i.e. G_{max} in Figure 5). However, as the strains increase, this relationship becomes non-linear causing soil stiffness to decrease, and damping to increase with strain. Figure 5 shows this typical stress-strain relationship where the stiffness is defined by the gradient of the solid black line and damping by the grey-shaded loop area. Secant and tangent stiffness formulations can be used to describe this behaviour, however the linear equivalent approach requires secant stiffness to be used.

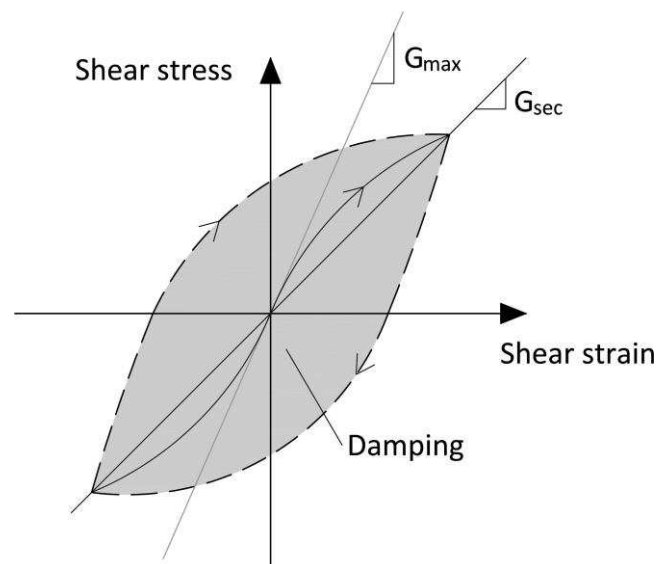


Figure 5: Strain-stress path during cyclic loading

To assess non-linear behaviour, a 'linear equivalent' approach is used. The advantage of using this is that it can be used with frequency domain approaches to reduce the computational demand in comparison to constitutive time domain models. By definition, it means that while the analysis remains linear, the soil properties are updated as function of the strain level, thus simulating non-linear type effects. It requires for the linear system of

equations to be computed, the strain levels assessed, the stiffness adjusted and the process repeated until convergence. It is implemented element-by-element (i.e. layer-by-layer) with the TLM formulation as follows:

1. Assume low strain properties for all thin-layer elements (i.e. G_{max} or G_0)
2. Compute strain time histories and effective octahedral shear strain within all elements using Equation 8
3. Use stiffness-strain relationship curves which are functions of confining stress and plasticity index, to update the stiffness within each element (Figure 10 (a))
4. Use damping-strain relationship curves which are functions of confining stress and plasticity index, to update the damping within each element (Figure 10 (b))
5. If the lower soil layer is unbound (i.e. infinite depth with no bedrock), update the absorbing layer to have identical properties to the deepest thin-layer element
6. Repeat steps 2 – 5 until the differences between shear modulus and damping of the central node in two consecutive iterations fall below the pre-defined convergence (i.e. 3% tolerance between iterations [15])

Plasticity index is typically determined using laboratory tests and effective octahedral strain is calculated as:

$$\gamma_{oct} = \alpha \frac{1}{3} \sqrt{(\epsilon_{xx} - \epsilon_{yy})^2 + (\epsilon_{xx} - \epsilon_{zz})^2 + (\epsilon_{yy} - \epsilon_{zz})^2 + 6(\gamma_{xy}^2 + \gamma_{xz}^2 + \gamma_{yz}^2)} \quad (8)$$

Where ϵ_{xx} , ϵ_{yy} and ϵ_{zz} are the strains in the three coordinate directions while γ_{xy} , γ_{yz} and γ_{xz} are the shear strains. These are calculated for all layers using Equation 5. α is a constant chosen as 0.65 in-line with other linear equivalent formulations [43].

3. Model validation

3.1 Soil stress validation

The linear equivalent formulation relies on the accurate calculation of stress and strain levels within the full depth of the soil layer. To show that the model is capable of computing these, results are compared against approximate values from the work of Chen et al. [44]. The benchmark problem consists of an Euler beam resting on a homogenous half-space, traversed by a 160kN moving vertical load at 30m/s. The beam is 4m wide, 0.3m thick and infinite in the direction of vehicle travel. Stresses are monitored at 2m directly below the soil surface, at the central line of the Euler beam. To simulate the problem, the beam is modelled analytically and the soil is modelled using the thin-layer method, with the equivalent stiffness computed as shown in the slab formulation (Equation 1). The material properties used for this simulation are shown in Table 1.

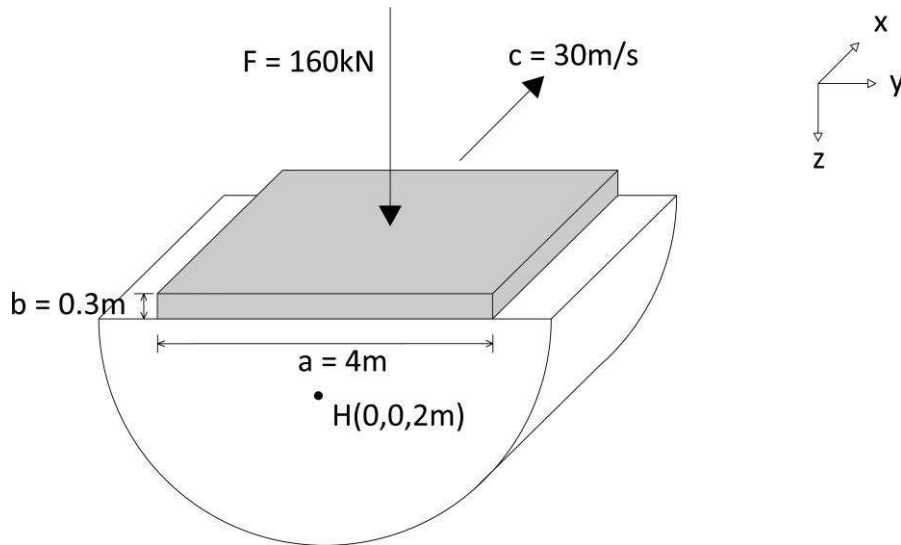


Figure 6: Schematic diagram of Chen's validation model

Table 1: Properties of the beam and the ground for Chen's validation

Beam			
Density (kg/m ³)	1900	Young's modulus (MPa)	30000
Width (m)	4	Thickness (m)	0.3
Mass (kg)	2280	Second moment of area (m ⁴)	0.009
Ground			
Density (kg/m ³)	1800	Young's modulus (MPa)	29
Poisson ratio	0.45	Shear wave speed (m/s)	74.54

Figure 7 shows a comparison of stress time histories between the published results and the result of the new TLM model. Four stress components are shown (σ_{xx} , σ_{yy} , σ_{zz} and τ_{xz}) because two of the shear stress components are zero (τ_{xy} and τ_{yz}) directly below the load. Strong agreement is seen between results with respect to both shape and magnitude. It should be noted that although this example validates stresses, the TLM formulation uses strain levels directly to compute stress levels, thus by default, also confirming the accuracy of strain levels. Therefore it can be concluded that the stress-strain computations within the soil model are accurate.

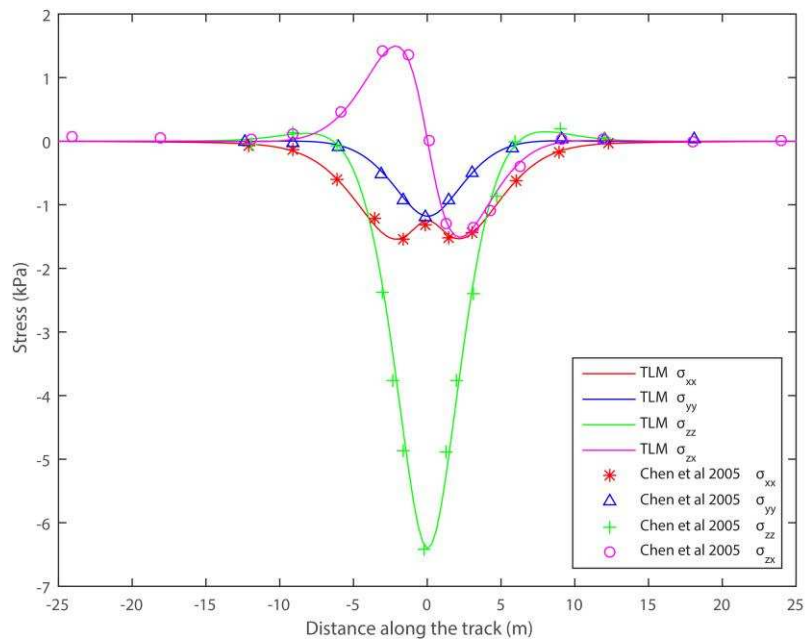


Figure 7: Comparisons of the dynamic stresses of an element at (0, 0, -2m) underneath the moving load

3.2 Experimental validation

The second validation is for field data recorded at Ledsgard, Sweden. This site was subject to large rail deflections and suspected high soil non-linearity during the passage of X2000 trains shortly after opening. This occurred because the track was constructed over soft ground, with a sandwiched layer of extremely soft organic clay (Figure 8). Therefore it has been used for a variety of numerical model validations (e.g. [2], [15], [38]).

The track is ballasted with the properties shown in Table 2, and rests on a 1.2m high embankment. The train is an X2000 with 5 carriages and 20 axle loads (Figure 9). Wheel-rail irregularities are not considered due to their minor influence on low-frequency dynamic track amplification. Also, it should be noted that although for the linear case the response of a single wheel can be used (i.e. via superposition) to compute the response of an entire train, this is not possible when considering soil non-linearity. Instead, for each run, the unique combination of train wheels is computed.

The soil properties at the site are shown in Table 3. All soil layers have a shear wave speed significantly lower than the engineered embankment, and the soil stratum is supported by bedrock at a depth of 30m. To model soil non-linearity, example shear modulus and damping ratio curves are shown in Figure 10, based upon triaxial tests performed on Ledsgard soil samples [15]. The shear modulus reduction curve formulations proposed by [45] require Plasticity Index (PI) and effective confining pressure (σ'_m) as inputs. Therefore [15] computed σ'_m at the centre of each physical soil layer, however in this work, these values are computed at the centre of each individual thin layer. This results in a much larger number (one per thin-layer element) of individual curves than the 4 examples shown in Figure 10.

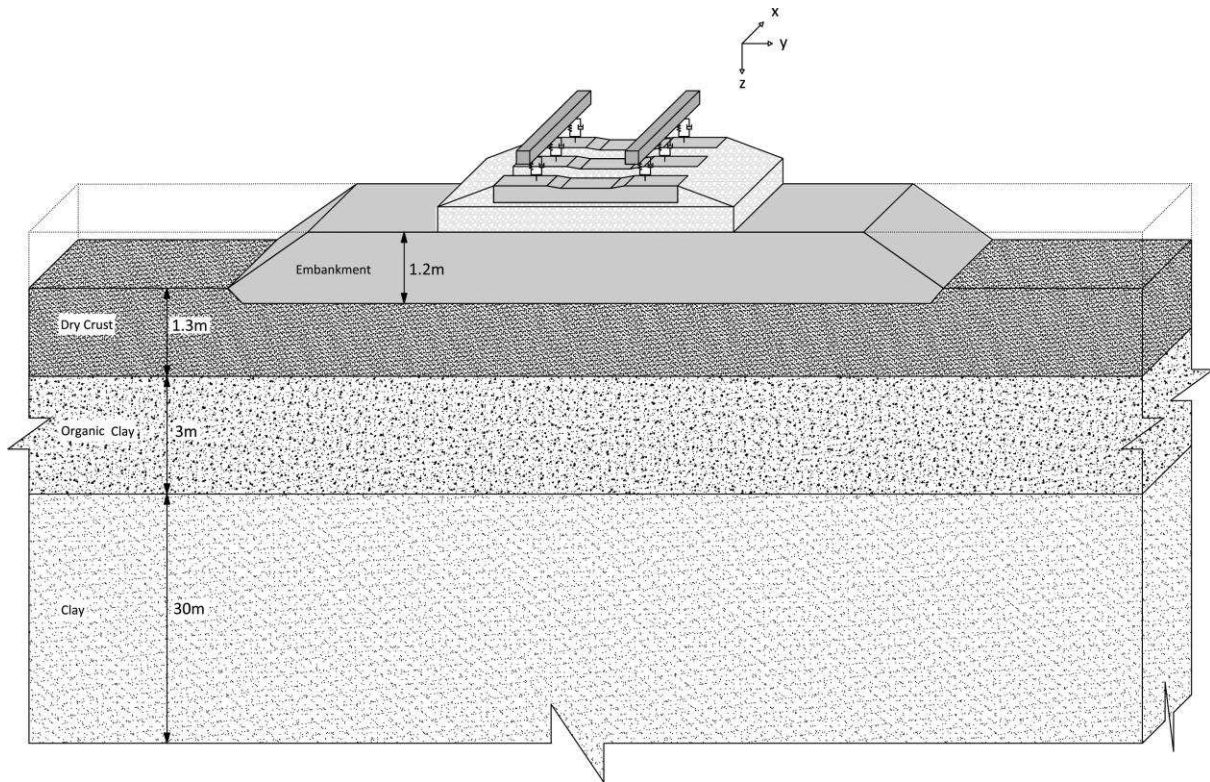


Figure 8: Geometric dimensions at the Ledsgard site

Table 2: Track parameters at the Ledsgard site

Rail	
Mass per unit length (kg/m)	120
Young's modulus (MN/m²)	210×10^3
Second moment of inertia (m⁴)	6.11×10^{-5}
Railpad	
Stiffness per unit length (MN/m)	350
Damping per unit length (kNs/m²)	30
Sleeper	
Mass per unit length (kg/m)	490
Ballast	
Density per unit length (kg/m³)	1200
Thickness of the ballast (m)	0.35
Ballast stiffness per unit length (MN/m²)	315
Compression wave speed in ballast (m/s)	786

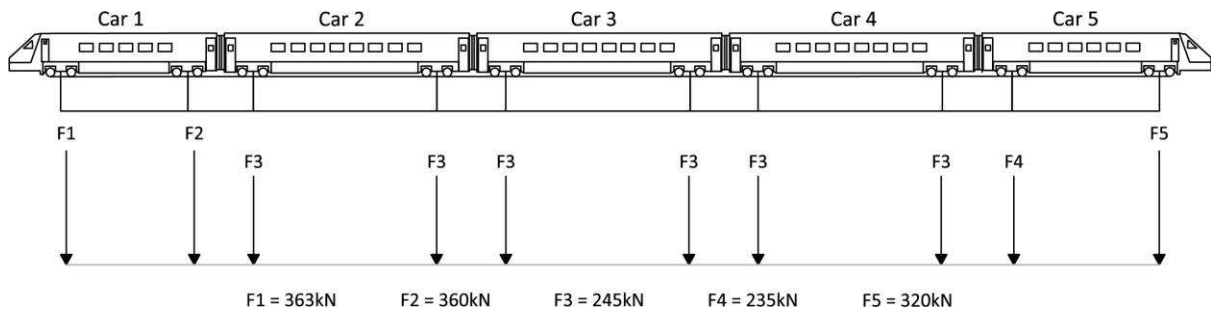


Figure 9: Geometric and mechanical properties of the X2000 train

Table 3: Low-strain properties of embankment and soil layers at the Ledsgard site

	Thickness (m)	P-wave speed (m/s)	S-wave speed (m/s)	Density (kg/m ³)	Damping
Embankment	1.2	340	210	1800	0.04
Dry crust	1.1	500	65	1500	0.04
Organic clay	3	500	40	1250	0.02
Clay	30	1500	87	1475	0.05

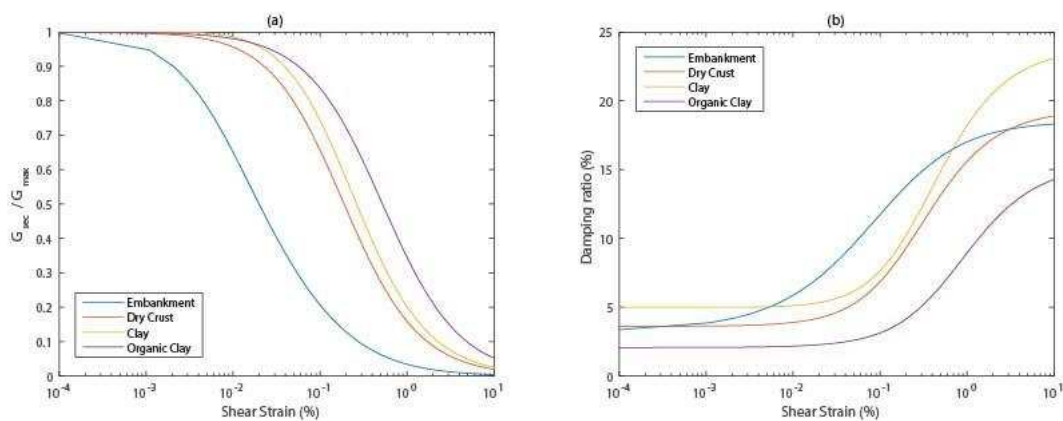


Figure 10: (a) Shear modulus reduction curves; (b) Damping ratio for different soil layers at Ledsgard [15]

Figure 11 (a), (b) and (c) compare the proposed model results with the field data for speeds of 70km/h, 140km/h and 180km/h, respectively. For speeds of 70 km/h and 140 km/h, the TLM model shows a match with the field data. For the higher speed of 180 km/h, there are a few small discrepancies, however overall a strong agreement in terms of shape and magnitude is found.

Figure 11 (d) compares the peak upward and downward rail deflections for the equivalent linear and linear simulation results. The positive values designate upward displacements and the negative values represent downward displacements.

At low speed the linear and equivalent linear simulations show a close match to each other. However, as speed increases, the equivalent linear results show larger deflections because the equivalent linear soil is less stiff in the presence of high strains, thus facilitating higher displacements. When compared to the field data, the equivalent linear results are a

closer match, with the linear case significantly underestimating maximum upward and downward deflections. This is particularly true as train speed approaches the critical velocity. For example, the maximum downward displacement at a speed of 180 km/h for the field data is 12.7mm. This is close to the equivalent linear predicted result of 13.3mm, but quite different to the linear value of 9.2mm. Therefore it can be concluded that the use of a non-linear formulation is necessary to accurately compute the track response.

Figure 12 (a) shows the degradation of the embankment surface shear modulus during the equivalent linear analysis. It is seen that it reduces by 38% after the 1st iteration, and after the convergence criteria has been met, it is only 46% of the original low-strain value. Further, Figure 12 (b) shows the Young's modulus versus depth for speeds of 70km/h and 204km/h. It can be seen that the reduction of embankment stiffness is approximately 50%, which matches with the result shown in Figure 12 (a). Also there is a large change to the Young's modulus in the top 2 soil layers (dry crust and organic clay layer). This indicates that they are undergoing high strains and their stiffness is degrading significantly as train speed increases. In contrast, as depth increases, strain levels decrease and train speed has little effect on Young's modulus.

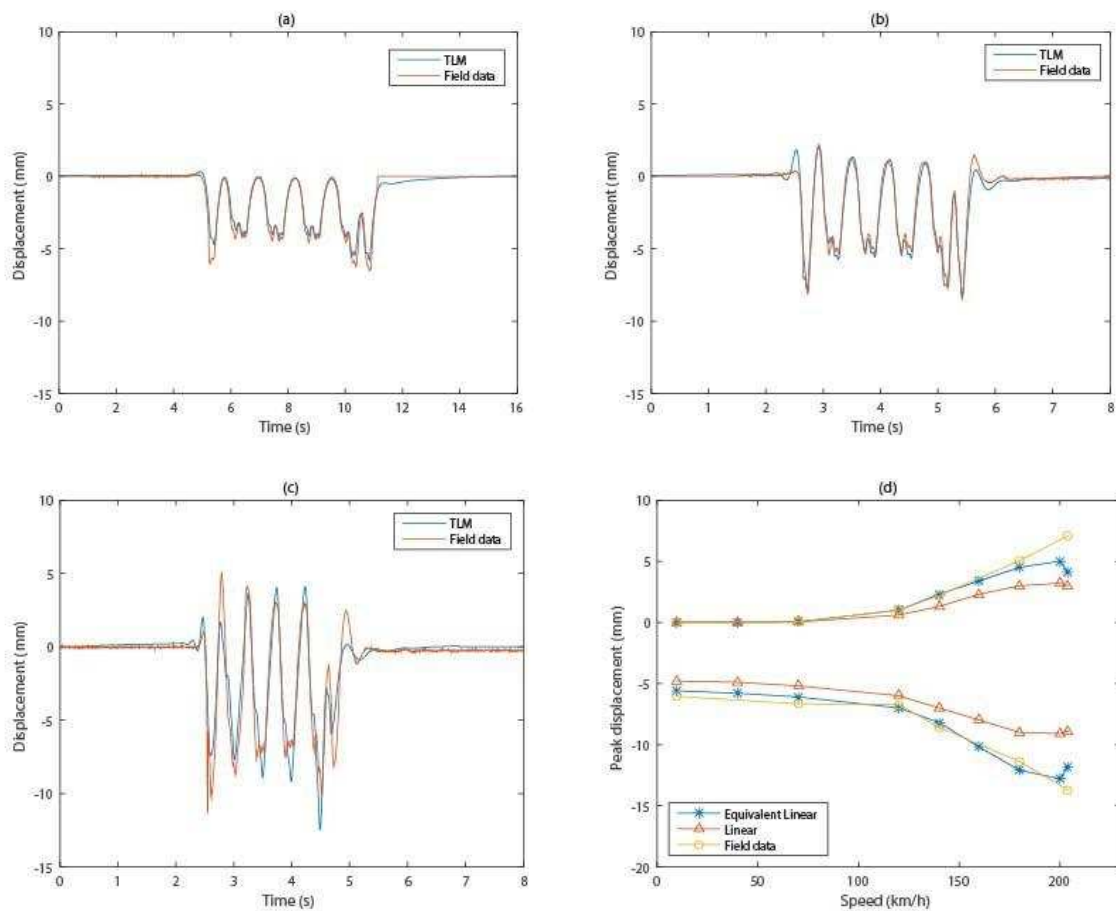


Figure 11: Measured and simulated time histories of track displacements for different train speeds: (a) $c=70\text{km/h}$; (b) $c=140\text{km/h}$; (c) $c=180\text{km/h}$; (d) Peak displacements versus train speeds (Southbound)

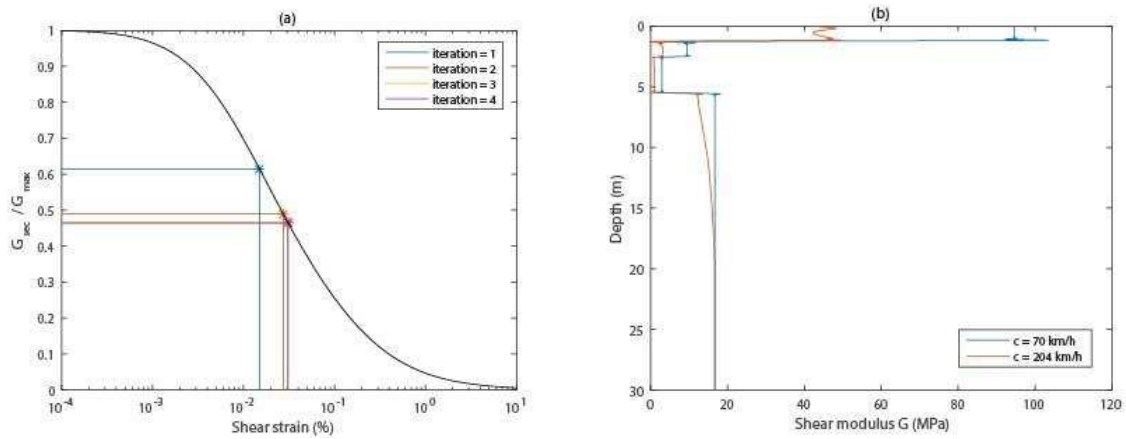


Figure 12: (a) Embankment shear modulus reduction process at each iteration step at speed of 204km/h; (b) Young's modulus comparison over the depth for speeds of 70km/h and 204km/h

Figure 13 shows the maximum octahedral shear strain versus depth for train speeds of 70km/h and 204km/h. It compares the linear and non-linear formulations, and also shows results published in [38], which were obtained using a comprehensive 3D constitutive model. The strain levels are low in the embankment due to its high stiffness but again the strains are large in the top 2 soil layers. As found previously, the strain levels are larger for the equivalent linear model compared to the linear model, particular towards the soil surface.

Comparing model results against [38], it is seen that strain levels are of similar magnitude. There are some discrepancies in the embankment and also towards the top of the clay layer. The discrepancy in the clay layer shows the strain levels in [38] decreasing more slowly than in the TLM model. This may be due to the different element sizes used in the different models – the TLM utilises much thinner elements, thus allowing non-linear effects to be captured more precisely. Furthermore, qualitatively comparing strains with depth against the contours presented in [15], in which an equivalent linear approach is applied on the basis of element-by-element strategy instead, strain levels are shown to decrease rapidly in-line with the TLM results.

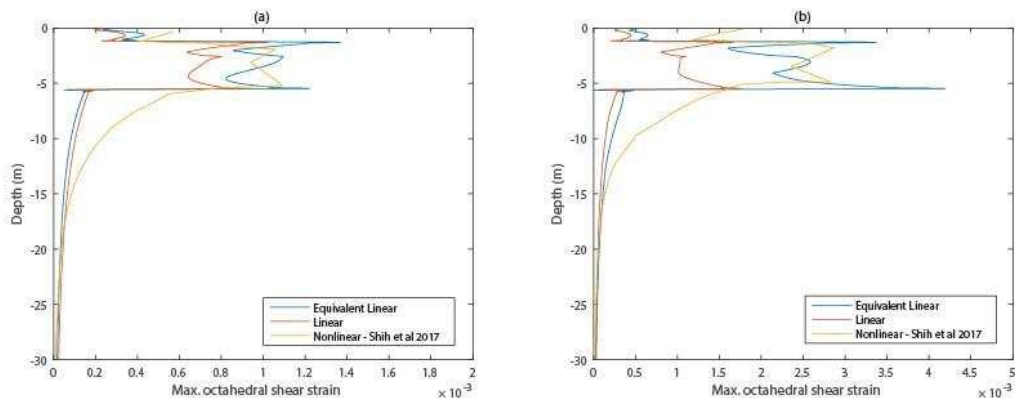


Figure 13: Variation of maximum octahedral shear strain with depth for train speed at (a) 70km/h; (b) 204km/h

4. Numerical analysis

As shown via the validation case, at high speed, railway lines can induce elevated subgrade strains which can result in non-linear soil behaviour. Therefore four soil case studies are undertaken, with properties shown in Table 4 and Figure 14, to investigate the effect of different soil stiffness's and layering combinations on track response. To account for non-linearity effect, the shear modulus degradation and damping ratio curves are based on the functions proposed by Ishibashi and Zhang [45]. Effective confining stress and plasticity index are governing factors that affect the non-linearity soil behaviour. In this study, the plasticity index is assumed to be 30 for all soils. In Figure 14, the corresponding primary wave speed C_p and secondary wave speed C_s of each soil layer are listed and two points (A and B), indicating upper and lower position of soil, are selected for each soil case for the strain analysis. The cases are:

1. A homogeneous low stiffness soil
2. A low stiffness soil overlying a stiffer soil
3. A high stiffness soil overlaying a softer soil
4. A homogeneous high stiffness soil

For all cases, the train is modelled as a moving 18 tonne axle load. A large number of train speeds are considered, as needed to plot dynamic amplification curves. Regarding the track, it is a ballasted track with properties shown in Table 5. A variety of output variables are plotted, however for dynamic amplification curves it should be noted that non-linear dynamic amplification is very sensitive to wheel spacing and therefore can change dramatically depending upon vehicle configuration.

Table 4: Soil properties used in the case studies

	Layer thickness (m)	Young's modulus (MPa)	Poisson's ratio	Density (kg/m³)	Damping
Soil 1	∞	45	0.35	1800	0.03
Soil 2	[2; ∞]	[45; 120]	[0.35; 0.35]	[1800; 1800]	[0.03; 0.03]
Soil 3	[2; ∞]	[100; 45]	[0.35; 0.35]	[1800; 1800]	[0.03; 0.03]
Soil 4	∞	200	0.35	1800	0.03

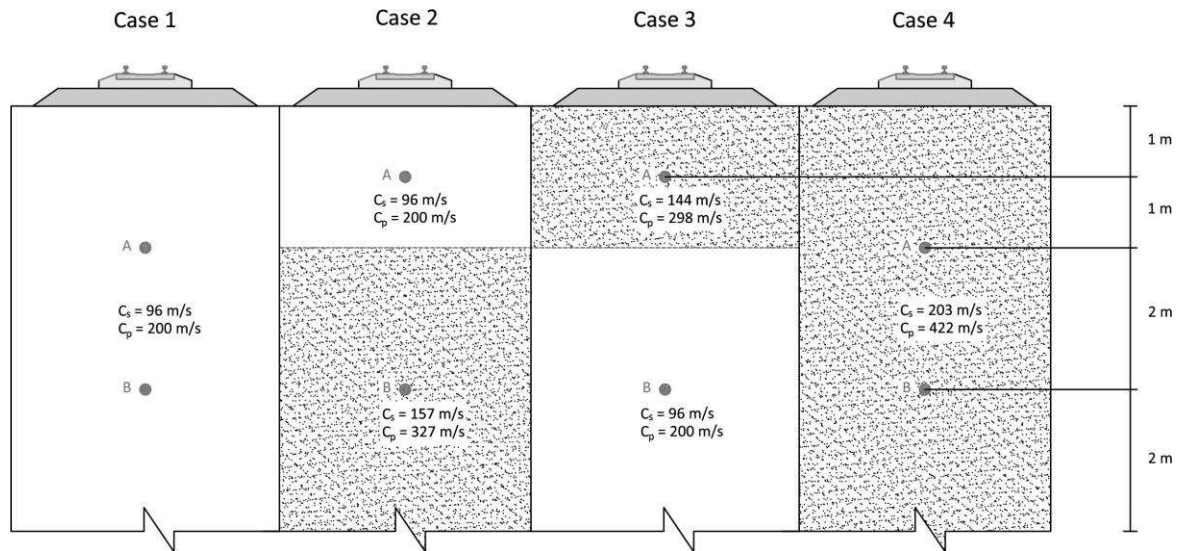


Figure 14: Wave speeds demonstration for different soil conditions

Table 5: Ballasted track properties

		Ballasted track
Rail	EL_r (Nm ²)	1.26×10^7
	m_r (kg/m)	120
Railpad	k_p (N/m)	5.5×10^8
	c_p (Ns/m)	2.5×10^5
Sleepers	m_s (kg/m)	490
Ballast	$h_{ballast}$ (m)	0.35
	$E_{ballast}$ (MPa)	150
	$2b$ (m)	2.5
	ρ (kg/m ³)	1600

4.1 Soil Case 1

Soil 1 is a homogeneous half-space with a Young modulus of 45MPa. Figure 15 shows the relationship between train speeds for four variables: a) rail displacement, b) ballast velocity, c) strain at 2m depth (Point A in Figure 14), and d) strain at 4m depth (Point B in Figure 14). The linear and non-linear results are compared for each, considering the passage of a single wheel. It should however be noted that for the non-linear case, the results are highly sensitive to wheel spacing and should be treated as indicative.

Firstly, considering rail displacements, the non-linear and linear curves have a similar shape. The linear case has lower displacements for the majority of speeds, except around its critical velocity peak at 90m/s. Regarding maximum dynamic amplification, the non-linear case shows 24.6% greater displacements compared to the linear case. Further, the critical velocity reduces from 91 m/s to 80 m/s. These effects occur because the soil stiffness is reduced for the equivalent linear case. This causes the track to deflect more, but

also lowers the wave propagation velocities, thus affecting the dispersive characteristics of the soil.

Analysing the octahedral strains at 2m and 4m below the ground surface shows a maximum at 91m/s, approximately the shear wave speed (and thus the critical velocity) of the linear soil case. However, for the non-linear case at 2m, the peak displacement magnitude increases by 20.8%, and the critical velocity shifts to 80 m/s which is 12.1% lower than the linear case. In comparison, at 4m the peak displacement magnitude increases by 10.1%, and the critical velocity shifts to 85 m/s which is 6.6% lower than the linear case. The effect at 2m is therefore more pronounced than at 4m and due to greater soil non-linearity close to the soil surface. This is further illustrated in Figure 16 which shows strain versus depth, for a low speed (10m/s) and the non-linear critical speed (80m/s). At a depth of 2m, strain levels are significantly higher than at 4m (2.4×10^{-4} vs 1.13×10^{-3}). Further, if a depth of 1m is considered, increasing the train speed results in a 387% increase in strain level.

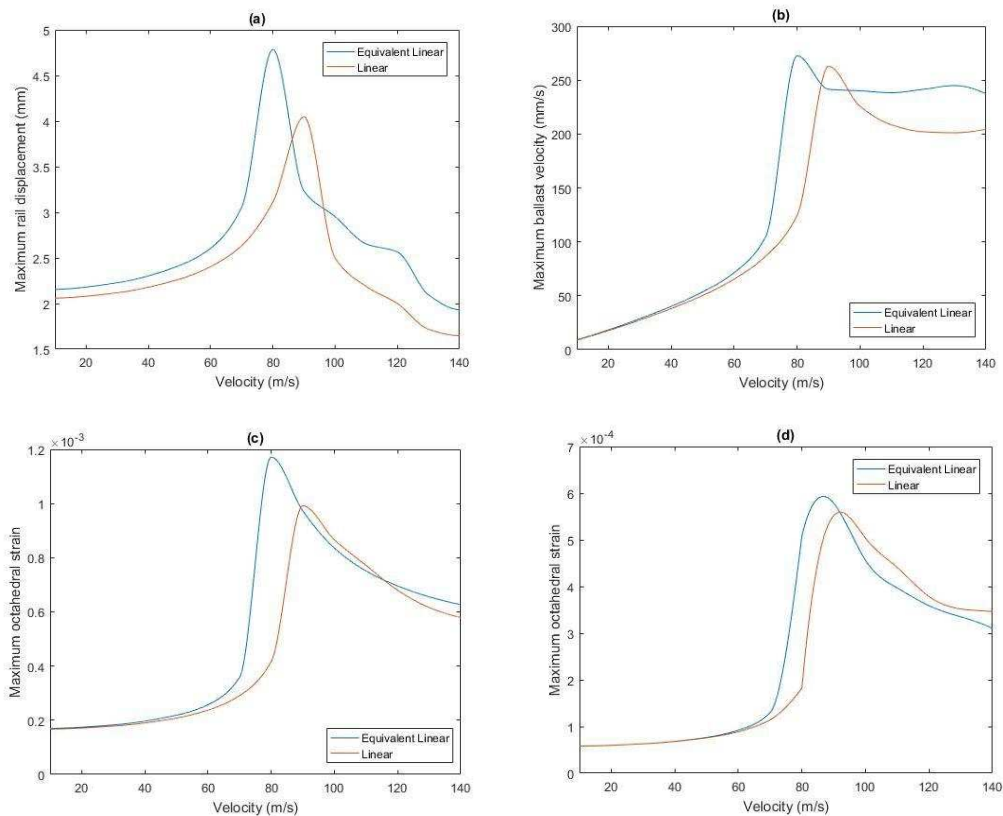


Figure 15: Soil case 1 comparisons of linear and equivalent nonlinear DAF curves of (a) rail displacements (b) ballast velocity (c) octahedral strain at Point A (d) octahedral strain at Point B

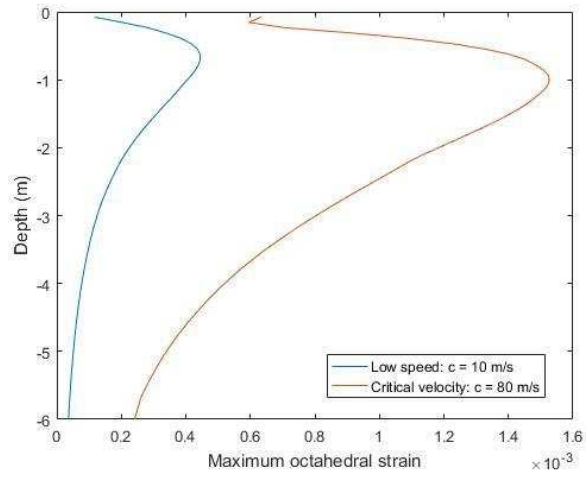
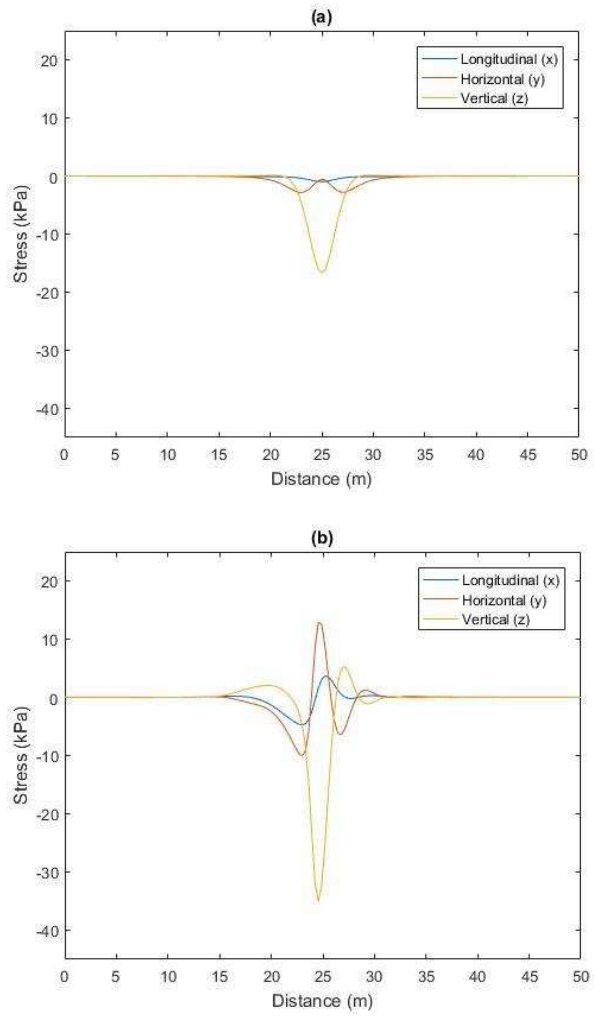


Figure 16: Maximum shear strain vs depth for $c = 10$ m/s and $c = 80$ m/s for non-linear Soil case 1



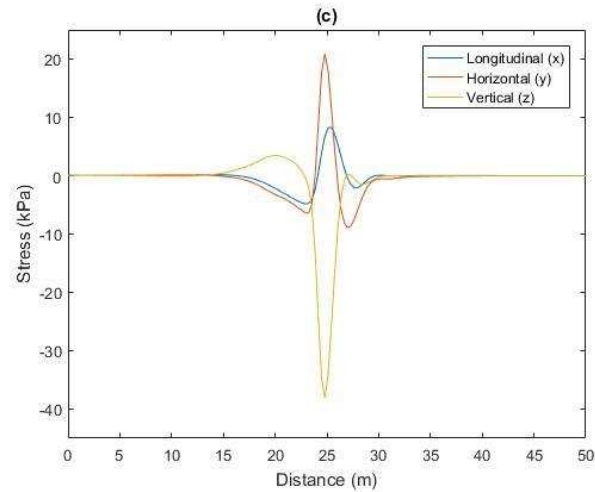


Figure 17: Stress history of Point A underneath the centre line of the track structure at the speeds of (a) $c = 10\text{m/s}$ (b) $c = 80\text{m/s}$ (c) $c = 130\text{m/s}$

Figure 17 shows the stress histories of the (non-linear) soil formulation at 2m depth (Point A), directly below the track for 3 speeds. At low speed, the stress history has a symmetrical shape and the magnitude of each stress component is small. However, as train speed increases, this symmetry is lost and all stress component magnitudes increase significantly. The change in magnitude is summarised in Table 6, where it is seen that higher speeds cause the horizontal stress component to increase as a proportion of the vertical stress. Therefore, although the vertical stress component increases with speed, when approaching the critical velocity, the horizontal components increase more rapidly. After experiencing a peak at 80m/s, all stresses components stabilise and only experience small additional increases. This is also shown in Figure 18 which shows the effect of speed on peak-peak stress components when considering soil non-linearity. In this figure it is seen that as train speed increases the discrepancy between vertical and horizontal stresses decreases.

Table 6: The magnitude of maximum stress components (peak-to-peak) at various speeds

	C = 10 m/s		C = 80 m/s		C = 130 m/s	
	Magnitude	Percentage	Magnitude	Percentage	Magnitude	Percentage
Vertical stress (kPa)	16.8	--	40.8	--	41.3	--
Horizontal stress (kPa)	2.8	16.7%	23.4	57.3%	30.1	72.8%
Longitudinal stress (kPa)	1.1	6.5%	9.1	22.3%	13.1	31.7%

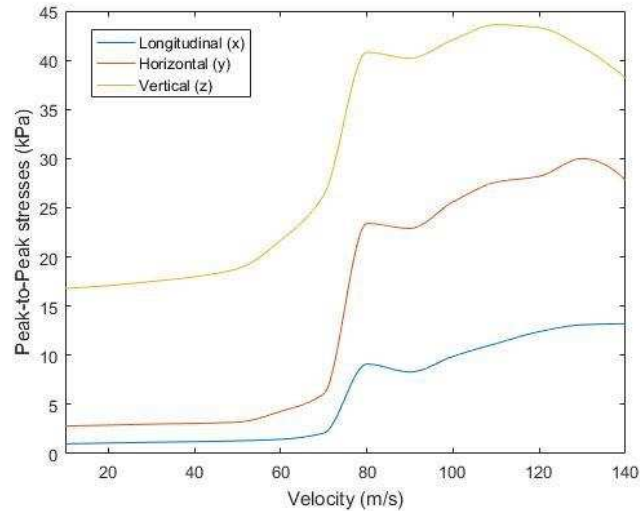


Figure 18: DAF curves for stress components at Point A in Soil case 1

4.2 Soil Case 2

Soil Case 2 consists of a 2m thick soft layer (45 MPa) overlying a stiffer homogenous half-space (120 MPa). Figure 19 (a) shows that the maximum rail displacement increases by 29.5%, from 2.95 mm to 3.82 mm, when considering soil stiffness degradation. In a similar manner to Soil Case 1, this is because the equivalent linear model results in decreased soil stiffness, therefore causing greater track deflections. However, in contrast to Case 1, track deflections are lower for the linear case for most of the train speeds, even at the linear critical speed.

Similarly, the critical speed shifts to 90 m/s, for the non-linear case, which represents a 20.0% decrease. This is due to the reduced wave speeds associated with the degraded soil stiffness. Additionally, the velocity-displacement gradient is very steep for the non-linear case immediately prior to critical velocity. This indicates that very minor changes to speed can almost double rail deflections. At speeds greater than the critical velocity, displacements reduce rapidly, to magnitudes even lower than the static load case. This is true for both the linear and non-linear case.

Figure 19 (b) shows the relationship between strain and soil depth for speeds of 10 m/s and 90 m/s, which represent the quasi-static case and also the non-linear critical velocity case. The black dotted line indicates the soft-stiff soil interface. The higher speed shows significantly larger strains compared to the low speed case, particularly in the top 2m where the softer soil is located. At the interface between the soft and stiff soils, there is a rapid reduction in strain levels for both speeds, however this is particularly pronounced for the higher speed. At the stiffer soil locations the strains remain higher for the non-linear case, however the values are lower than in the soft soil layer, and converge rapidly until a depth of approximately 6m.

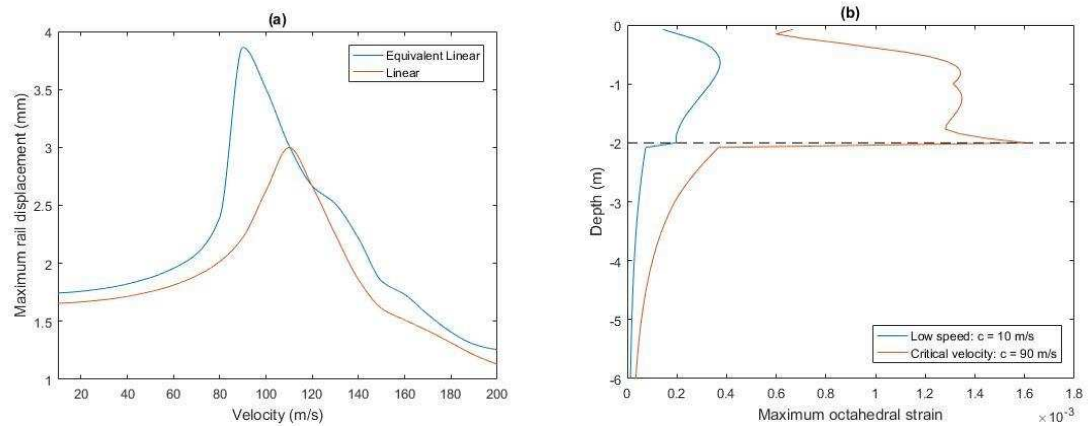


Figure 19: Soil case 2, (a) comparisons of linear and nonlinear DAF rail displacement curves, (b) Maximum (non-linear) shear strain vs depth for $c = 10$ m/s and $c = 90$ m/s

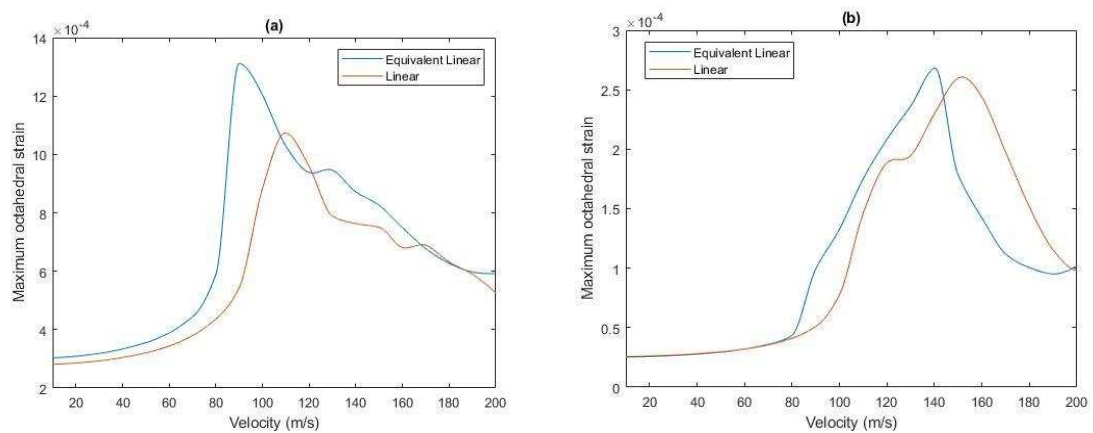


Figure 20: Soil case 2 comparisons of linear and nonlinear DAF curves of maximum octahedral strain (a) at Point A (b) at Point B

Figure 20 compares octahedral strain dynamic amplification curves for the linear and non-linear formulations, at depths of both 1m (Point A) and 4m (Point B) below the soil surface. The 1m location represents the centre of the soft layer, while the 4m location represents a depth 2m below the soft-stiff layer interface. Figure 20 (a) shows that the peak strain of the linear result at 1m is located at 110 m/s, which is close to the linear track-ground critical velocity. Similarly, for the 4m case, the peak (low-strain) strains are found at 152m/s, corresponding to the shear wave velocity of the lower layer. Therefore the critical velocity is located between the speeds of peak strains in both layers. This is in contrast to Soil Case 1, where the critical velocity at all soil and track locations (in terms of either strain or displacement), is constant. This is because P-SV waves are non-dispersive for Soil Case 1, while in Soil Case 2 P-SV waves experience dispersion due to the presence of two contrasting stiffness soil layers.

Comparing the linear and non-linear cases, the maximum strain levels are elevated by 23.4% and 5.3% when non-linearity is considered, for the 1m and 4m locations respectively. Further, the critical speeds are shifted by 18.2% and 10.7% respectively. Interestingly, for the 1m case, for the majority of train speeds, the strains are higher for the non-linear case, however at 4m between speeds of 140-200m/s, the linear case shows higher displacements.

Further, at low train speed, there is discrepancy between the linear and non-linear cases at 1m, however at a depth of 4m, below a speed of 70m/s, both formulations result in almost identical strain magnitudes. This is because strains reduce with depth, meaning the deeper soil locations are less susceptible to soil stiffness degradation.

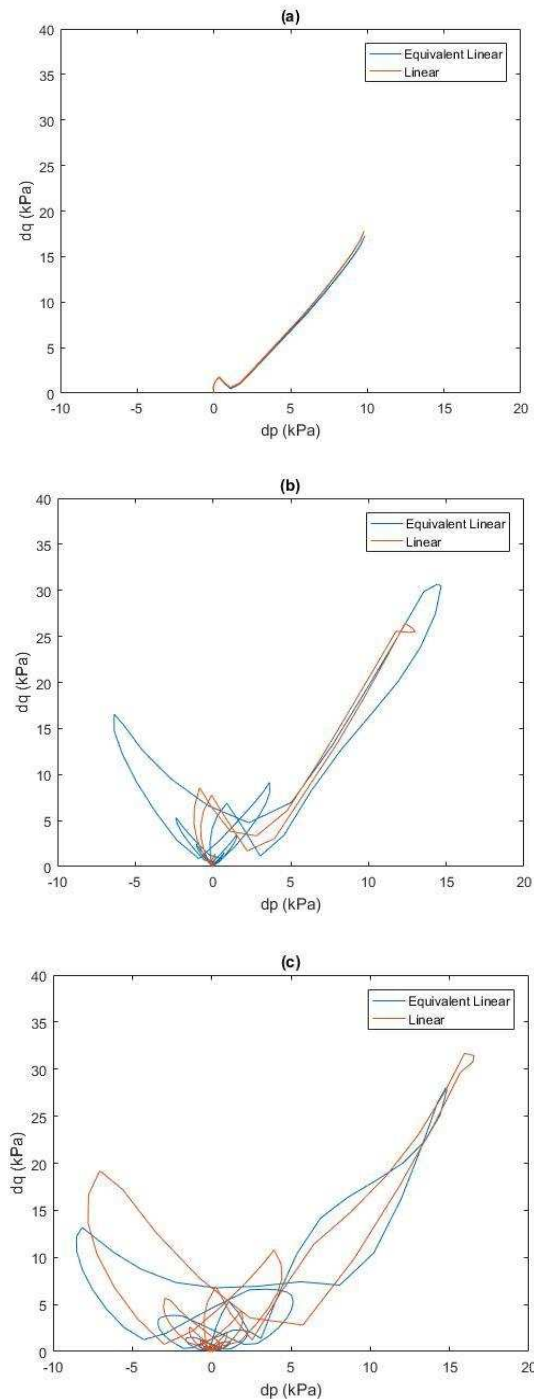


Figure 21: Stress path followed at point A during the load passage with different speeds (a) $c = 10$ m/s (b) $c = 90$ m/s (c) $c = 110$ m/s

Figure 21 shows the p-q stress paths at a depth of 1m below the track centre-line for speeds of 10, 90 and 110 m/s. The stress paths are computed using the mean stress increment (dp) and shear stress increment (dq):

$$dp = \frac{\Delta\sigma_1 + \Delta\sigma_2 + \Delta\sigma_3}{3}$$

$$dq = \sqrt{\frac{(\Delta\sigma_1 - \Delta\sigma_2)^2 + (\Delta\sigma_1 - \Delta\sigma_3)^2 + (\Delta\sigma_2 - \Delta\sigma_3)^2}{2}}$$

Where σ_1, σ_2 and σ_3 represent the principal stresses. At a speed of 10m/s, there is no sign of dynamic amplification. However, when the speed is 110 m/s, (i.e. close to the critical velocity), the stress state becomes highly turbulent and the magnitudes increase significantly. This is consistent with the findings of [46].

4.3 Soil Case 3

Soil Case 3 consists of a stiffer 2m layer (100MPa) overlying a softer lower layer (45MPa). It is therefore an inversely dispersive scenario, where phase velocities both increase and decrease depending upon frequency.

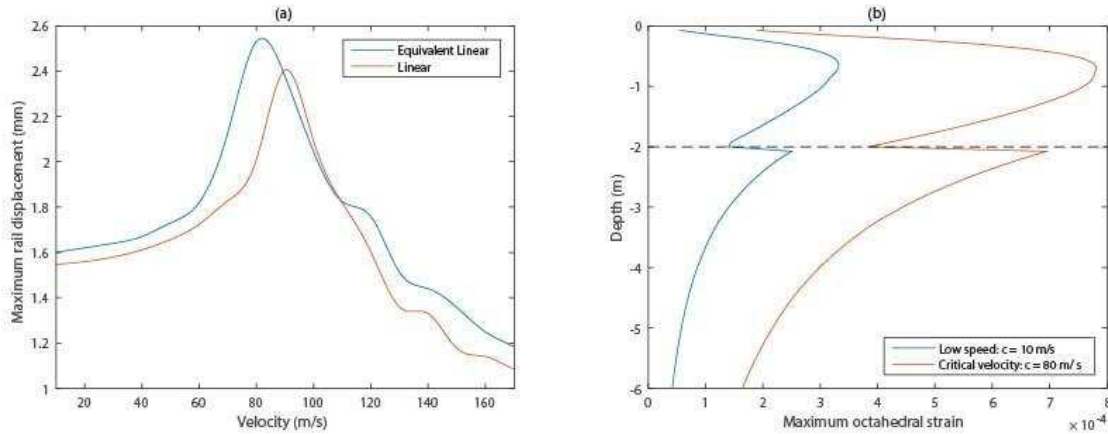


Figure 22: Soil case 3, (a) comparisons of linear and nonlinear DAF rail displacement curves,(b) Maximum (non-linear) shear strain vs depth for $c = 10$ m/s and $c = 80$ m/s

Figure 22 shows the effect of moving speed on maximum rail displacement. The non-linear formulation results in a 7.2% increase in maximum displacement and 11.3% critical velocity respectively. These discrepancies are lower in magnitude compared to the previous soil case, and are due to the stiffer soil being located near the surface. This results in lower strain levels near the soil surface, and that decay less rapidly with depth. For example, for Soil Case 2, Figure 19 shows a maximum strain in the top 2m of 1.32×10^{-3} , and a maximum of 3.1×10^{-4} in the lower layer (i.e. 325% reduction). In contrast, for Soil Case 3, Figure 22 shows that the maximum strains in the upper and lower layers are 7.8×10^{-4} and 6.8×10^{-4} respectively, which is a 14.7% reduction. Therefore the upper soil layer has less influence on overall non-linearity for Case 3 compared to Case 2. Another notable difference between these cases is that for case 2, strains reduce dramatically when moving across the upper to lower layer interface. In contrast, Case 3 (Figure 22) shows that strains increase (but less drastically) when crossing the upper to lower layer interface. This occurs because softer soil layers typically experience higher strain levels.

Figure 22 (a) also shows displacement oscillations at speeds greater than the critical velocity for the linear case. The critical speed computed using the linear analysis is located at 90 m/s which is related to the lower layer shear wave speed, while the second peak is at 136 m/s, and thus coincides with the shear wave velocity of the upper soil layer.

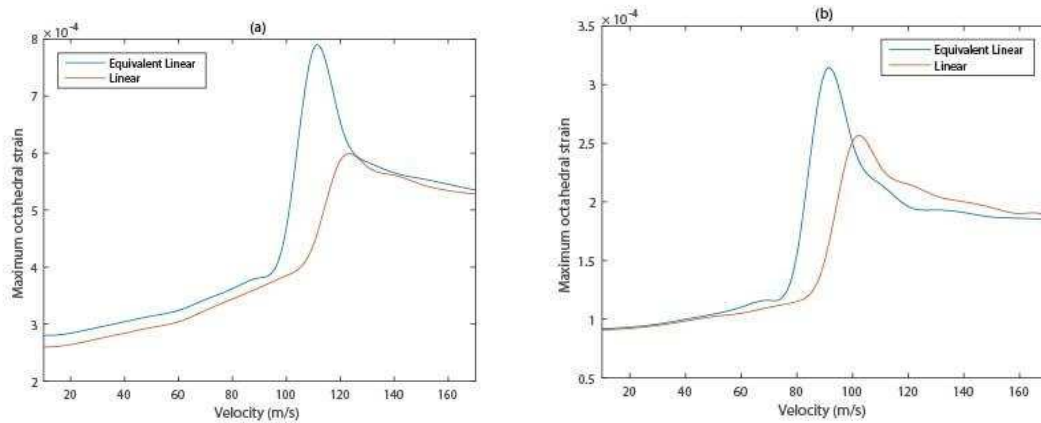
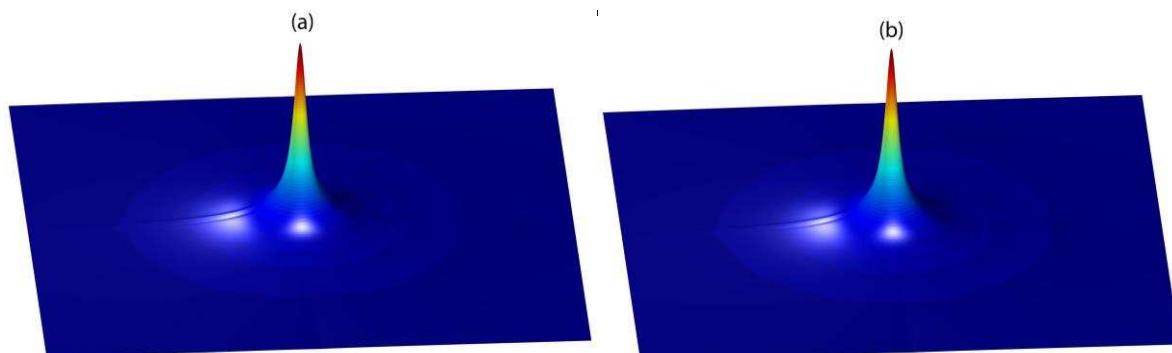


Figure 23: Soil case 3 comparisons of linear and nonlinear DAF curves of maximum octahedral strain (a) at Point A (b) at Point B

Figure 23 shows the relationship between maximum octahedral strain and train speed, for both soil formulations and at depths of 1m and 4m below the track. For the non-linear case at both depths, there is a more pronounced increase and decrease in strain levels immediately before/after the peak strain values. These peaks are 8.3% and 11.5% lower than the linear case, in terms of critical velocity respectively, but the magnitudes are 30.7% and 27.8% higher than the linear result. Although, for all cases, strain levels are lower than those for Case 2, at higher speeds, the decrease in strain levels at very high speed is also lower than Case 2. Interestingly, at very low and very high speeds, strain levels are similar for the linear and non-linear cases. The main discrepancy occurs in a localised speed range close to the critical velocity where the amplification effects are more dominant.

Considering the linear cases, the peak values do not correspond to the shear wave speeds of either the upper or lower supporting soil. This difference is caused by the complex dispersion characteristics of the inversely-dispersive profile.



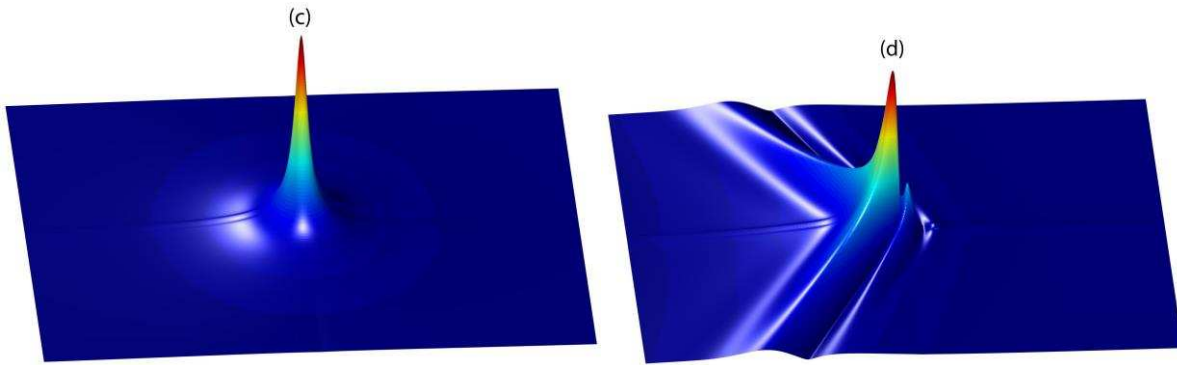


Figure 24: Normalised ground surface contours (a) Linear: $c = 10 \text{ m/s}$ (b) Nonlinear: $c = 10 \text{ m/s}$ (c) Linear: $c = 80 \text{ m/s}$ (d) Nonlinear: $c = 80 \text{ m/s}$

Finally, Figure 24 shows ground surface contour plots for high (80m/s) and low (10m/s) speed wheel passages, computed using both linear and non-linear formulations. At low speed, the soil response is uniform and symmetrical, and the contours for the linear and non-linear formulations are similar. However, at high speed, the linear and non-linear responses are markedly different. The linear formulation is relatively uniform and similar to both low speed responses, however, the non-linear result has a significantly pronounced wavefront. This occurs because the moving load speed is at the critical velocity of the non-linear soil (i.e. degraded stiffness soil), while it is below the linear critical velocity. Therefore it can be concluded that track-ground behaviour can be markedly different when considering linear and non-linear soil behaviour.

4.4 Soil Case 4

Soil Case 4 is a homogeneous half-space, similar to Case 1, however with a greater stiffness ($E=200\text{MPa}$). Figure 25 (a) shows the relationship between rail displacement and train speed, where it is seen that the curve shape for both formulations is similar. However, the non-linear formulation shows a 1.3% increase in maximum displacement and 15.8% decrease and critical velocity respectively. Although the change in critical speed is comparable to Case 1, the increase in magnitude is significantly different (20.7% for case 1). Also, for Case 1, rail displacements at low speed are greater for the non-linear case, however when the soil has a Young modulus of 200 MPa, the displacements are almost identical at speeds below 70m/s. This occurs because the elevated stiffness results in the generation of lower strains inside the soil stratum. This is seen in Figure 25 (b) which compares strain with depth for low speed (10m/s) and at the non-linear critical velocity (150m/s). The high speed case exhibits higher maximum strain levels (4.24×10^{-4} compared to 1.92×10^{-4} for the low speed case). However, these are still relatively low, meaning soil stiffness degradation is also low.

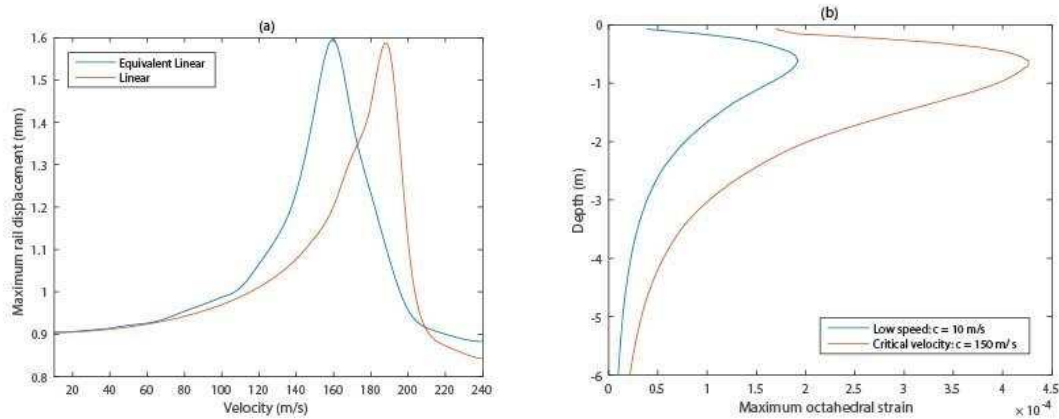


Figure 25: Soil case 4, (a) comparisons of linear and nonlinear DAF rail displacement curves (b) Maximum (non-linear) shear strain vs depth for $c = 10$ m/s and $c = 150$ m/s

5. Discussion

The four case studies presented show that train speed has a marked effect on track-ground response during train passage. Table 7 summaries the results and shows that dynamic track deflections increase with speed from their static value by between 58% and 120%.

Further, Table 7 quantifies the large discrepancy between track displacements computed using linear and non-linear formulations. This discrepancy is up to 30% for the case of a soft soil overlying a stiffer soil, however is less of a problem when the entire soil layer is stiff. Table 7 also shows that the critical speed is influenced when considering non-linearity. For all soil cases, the critical velocity is shifted to a lower value, ranging between 80-89% of the original linear value. Also, at speeds close-to, but below the critical velocity, the non-linear formulation reveals that the gradient of the dynamic amplification curve is much steeper with respect to speed compared to the linear case.

These two findings are important when designing high speed lines because often 70% of the linear critical speed is chosen as the cut-off track-foundation design criteria. Therefore, if the railway track/foundations are designed to have a critical speed ≈ 50 -70% of the linear value, the track may be of risk of high dynamic effects. As an example, case 2 shows a very steep velocity-displacement gradient immediately prior to the critical velocity, indicating small speed changes will radically alter track deflections. Therefore this could be problematic if it is decided to increase train speeds slightly in the future.

It should be noted that the reduction in critical speed is dependent upon the characteristics of the soil, because the non-linear stiffness degradation of cohesive and granular soils is very different. Cohesive soils have plasticity and the sensitivity of their shear stiffness degradation curves to the confining stress is low. Alternatively, granular soils have a low plasticity index and are more greatly affected by confining stress. In practical railway situations, embankments are typically constructed using granular materials while the underlying soil might be cohesive. Therefore, in addition to the train-induced stresses,

embankment stiffness degradation will be effected by confining stress, while the supporting soil might be more greatly effected by plasticity index.

It should also be noted that although this research presents dynamic amplification curves considering subgrade non-linearity, the results are for a single wheel passage only. This is acceptable for linear simulations, however for non-linear ones, the results can be greatly affected by vehicle axle configuration (i.e. axle spacing) and, the axle load. Therefore, when investigating the effect of subgrade non-linearity in practise, rolling stock configuration should be considered since it has a strong influence on track-ground behaviour.

Finally, stiffness degradation and consequently the reduction of the critical speed can have a strong impact on the accumulation of permanent strains in the ground. This can be investigated using shakedown limit analysis, such as that presented by [46].

Table 7: Summary of effect of non-linearity on rail displacements and critical velocity

	Rail displacement		Critical speed
	<i>Percentage increase from maximum linear displacement</i>	<i>Percentage increase from static displacement</i>	<i>Percentage decrease from linear speed</i>
Soil Case 1	24.6%	114.5%	12.2%
Soil Case 2	29.5%	120.5%	20.0%
Soil Case 3	7.2%	58.1%	11.3%
Soil Case 4	1.3%	77.4%	15.8%

6. Conclusions

This paper presents a frequency domain numerical model to investigate the effect of soil non-linearity on the response of high speed railway lines. The model uses analytical expressions to describe the response of the track and a thin-layer element method for the ground. The model is coupled with a 'linear equivalent' formulation to allow the soil stiffness to change depending upon strain level. The linear stress-strain implementation is validated using an independently published dataset and the non-linear response is validated using field data collected on a high-speed railway line. The model is used to investigate four railway case studies, each with highly contrasting subgrade characteristics. It is found that non-linearity has a very significant influence on track-ground response. For example, the critical velocity shifts to as low as 80% of the linear case, while rail deflections are up to 30% higher. Further, at speeds close-to, but below, the non-linear critical velocity, dynamic amplification is highly sensitive to small increases in train speed. These findings depend upon material properties, and are important for high speed rail track-earthwork designers because often 70% of the linear critical velocity is used as a design limit. However, this work shows that designs close to this limit may be still at risk of high dynamic effects, particularly if line speed is increased slightly at a later date.

Acknowledgements

The authors are grateful to Heriot Watt University, the University of Leeds and the University of Porto for facilitating this research. Financial support from the Leverhulme Trust (UK) is also gratefully acknowledged. In addition, the participation of last author was financially supported by: Project POCI-01-0145-FEDER-007457 – CONSTRUCT – Institute of R&D In Structures and Construction funded by FEDER funds through COMPETE2020 – Programa Operacional Competitividade e Internacionalização (POCI) – and by national funds through FCT – Fundação para a Ciência e a Tecnologia; Project POCI-01-0145-FEDER-029577 – funded by FEDER funds through COMPETE2020 – Programa Operacional Competitividade e Internacionalização (POCI) and by national funds (PIDDAC) through FCT/MCTES.

References

- [1] V. V. Krylov, "Generation of ground vibrations by superfast trains," *Appl. Acoust.*, vol. 44, no. 2, pp. 149–164, 1995.
- [2] C. Madshus and A. M. Kaynia, "High-Speed Railway Lines on Soft Ground: Dynamic Behaviour At Critical Train Speed," *J. Sound Vib.*, vol. 231, no. 3, pp. 689–701, 2000.
- [3] A. M. Kaynia, C. Madshus, and P. Zackrisson, "Ground vibration from high-speed trains: Prediction and countermeasure," *J. Geotech. Geoenvironmental Eng.*, vol. 126, no. 10, pp. 531–537, 2000.
- [4] H. Lamb, "On the propagation of tremors over the surface of an elastic solid," *Philos. Trans. R. Soc. London*, vol. 203, pp. 1–42, 1904.
- [5] L. Fryba, *Vibration of Soilds and Structures under Moving Loads*. Springer Netherlands, 1972.
- [6] H. a. Dieterman and a. V. Metrikine, "The equivalent stiffness of a half-space interacting with a beam. Critical velocities of moving load along the beam," *Eur. J. Mech. A/Solids*, vol. 15, pp. 67–90, 1996.
- [7] X. Sheng, C. J. C. Jones, and D. J. Thompson, "A comparison of a theoretical model for quasi-statically and dynamically induced environmental vibration from trains with measurements," *J. Sound Vib.*, vol. 267, no. 3, pp. 621–635, 2003.
- [8] D. Thompson, *Railway noise and vibration: mechanisms, modelling and means of control*. Elsevier, 2008.
- [9] P. Alves Costa, A. Colaço, R. Calçada, and A. Silva Cardoso, "Critical speed of railway tracks. Detailed and simplified approaches," *Transp. Geotech.*, vol. 2, pp. 30–46, 2015.
- [10] E. Kausel and J. M. Roesset, "Stiffness matrices for layered soils," *Bull. Seismol. Soc. Am.*, vol. 71, no. 6, pp. 1743–1761, 1981.
- [11] X. Bian, C. Cheng, J. Jiang, R. Chen, and Y. Chen, "Numerical analysis of soil vibrations due to trains moving at critical speed," *Acta Geotech.*, vol. 11, no. 2, pp. 281–294, 2016.

- [12] K. Dong, D. P. Connolly, O. Laghrouche, P. K. Woodward, and P. Alves Costa, "The Stiffening of Soft Soils on Railway Lines," *Transp. Geotech.*, vol. 17, pp. 178–191, 2018.
- [13] P. Alves Costa, "Vibrações Do Sistema Via-Macizo Induzidas Por Tráfego Ferroviário . Modelação Numérica E Validação Experimental", PhD Thesis, Faculty of Engineering, University of Porto, 2011.
- [14] A. Colaço, P. Alves Costa, and D. . Connolly, "The influence of train properties on railway ground vibrations," *Struct. Infrastruct. Eng.*, vol. 12, no. 5, pp. 517–534, 2016.
- [15] P. Alves Costa, R. Calçada, A. Silva Cardoso, and A. Bodare, "Influence of soil non-linearity on the dynamic response of high-speed railway tracks," *Soil Dyn. Earthq. Eng.*, vol. 30, no. 4, pp. 221–235, 2010.
- [16] P. Galvín, D. L. Mendoza, D. P. Connolly, G. Degrande, G. Lombaert, and A. Romero, "Scoping assessment of free- field vibrations due to railway traffic," *Soil Dyn. Earthq. Eng.*, vol. 114, pp. 598–614, 2018.
- [17] X. . Bian, Y. . Chen, and T. Hu, "Numerical simulation of high-speed train induced ground vibrations using 2.5D finite element approach," *Sci. China Ser. G Phys. Mech. Astron.*, vol. 51, no. 6, pp. 632–650, 2008.
- [18] S. François, M. Schevenels, P. Galvín, G. Lombaert, and G. Degrande, "A 2.5D coupled FE-BE methodology for the dynamic interaction between longitudinally invariant structures and a layered halfspace," *Comput. Methods Appl. Mech. Eng.*, vol. 199, no. 23–24, pp. 1536–1548, 2010.
- [19] P. Galvín, S. François, M. Schevenels, E. Bongini, G. Lombaert, and G. Degrande, "A 2.5D coupled FE-BE methodology for the prediction of railway induced vibrations," *Soil Dyn. Earthq. Eng.*, vol. 30, pp. 1500–1512, 2010.
- [20] H. Chebli, R. Othman, and D. Clouteau, "Response of periodic structures due to moving loads," *Comptes Rendus - Mec.*, vol. 334, no. 6, pp. 347–352, 2006.
- [21] H. Chebli, D. Clouteau, and L. Schmitt, "Dynamic response of high-speed ballasted railway tracks: 3D periodic model and in situ measurements," *Soil Dyn. Earthq. Eng.*, vol. 28, no. 2, pp. 118–131, 2008.
- [22] H. Chebli, R. Othman, D. Clouteau, M. Arnst, and G. Degrande, "3D periodic BE-FE model for various transportation structures interacting with soil," *Comput. Geotech.*, vol. 35, no. 1, pp. 22–32, 2008.
- [23] E. Arlaud, S. Costa D'Aguiar, and E. Balmes, "Validation of a reduced model of railway track allowing long 3D dynamic calculation of train-track interaction," *Comput. Methods Recent Adv. Geomech. - Proc. 14th Int. Conf. Int. Assoc. Comput. Methods Recent Adv. Geomech. IACMAG 2014*, no. September, pp. 1193–1198, 2015.
- [24] Y. B. Yang, H. H. Hung, and D. W. Chang, "Train-induced wave propagation in layered soils using finite/infinite element simulation," *Soil Dyn. Earthq. Eng.*, vol. 23, no. 4, pp. 263–278, 2003.
- [25] P. Galvín and J. Domínguez, "Analysis of ground motion due to moving surface loads

- induced by high-speed trains," *Eng. Anal. Bound. Elem.*, vol. 31, no. 11, pp. 931–941, 2007.
- [26] P. Galvin, A. Romero, and J. Domínguez, "Fully three-dimensional analysis of high-speed train-track-soil-structure dynamic interaction," *J. Sound Vib.*, vol. 329, no. 24, pp. 5147–5163, 2010.
- [27] L. Auersch, "The excitation of ground vibration by rail traffic: Theory of vehicle-track-soil interaction and measurements on high-speed lines," *J. Sound Vib.*, vol. 284, no. 1–2, pp. 103–132, 2005.
- [28] J. O'Brien and D. C. Rizos, "A 3D BEM-FEM methodology for simulation of high speed train induced vibrations," *Soil Dyn. Earthq. Eng.*, vol. 25, no. 4, pp. 289–301, 2005.
- [29] L. Hall, "Simulations and analyses of train-induced ground vibrations in finite element models," *Soil Dyn. Earthq. Eng.*, vol. 23, no. 5, pp. 403–413, 2003.
- [30] D. Connolly, A. Giannopoulos, and M. C. Forde, "Numerical modelling of ground borne vibrations from high speed rail lines on embankments," *Soil Dyn. Earthq. Eng.*, vol. 46, pp. 13–19, 2013.
- [31] D. Connolly, A. Giannopoulos, W. Fan, P. K. Woodward, and M. C. Forde, "Optimising low acoustic impedance back-fill material wave barrier dimensions to shield structures from ground borne high speed rail vibrations," *Constr. Build. Mater.*, vol. 44, pp. 557–564, 2013.
- [32] G. Kouroussis, O. Verlinden, and C. Conti, "Free field vibrations caused by high-speed lines: Measurement and time domain simulation," *Soil Dyn. Earthq. Eng.*, vol. 31, no. 4, pp. 692–707, 2011.
- [33] A. El Kacimi, P. K. Woodward, O. Laghrouche, and G. Medero, "Time domain 3D finite element modelling of train-induced vibration at high speed," *Comput. Struct.*, vol. 118, pp. 66–73, 2013.
- [34] J. N. Varandas, A. Paixão, E. Fortunato, and P. Hölscher, "A Numerical Study on the Stress Changes in the Ballast Due to Train Passages," *Procedia Eng.*, vol. 143, no. Ictg, pp. 1169–1176, 2016.
- [35] J. Chen and Y. Zhou, "Dynamic responses of subgrade under double-line high-speed railway," *Soil Dyn. Earthq. Eng.*, vol. 110, no. August 2017, pp. 1–12, 2018.
- [36] B. Oliver, D. Connolly, P. Alves Costa, and G. Kouroussis, "The effect of embankment on high speed rail ground vibrations," *Int. J. Rail Transp.*, vol. 4, no. 4, pp. 229–246, 2016.
- [37] G. Kouroussis, D. P. Connolly, K. Vogiatzis, and O. Verlinden, "Modelling the environmental effects of railway vibrations from different types of rolling stock: A numerical study," *Shock Vib.*, vol. 2015, 2015.
- [38] J. Y. Shih, D. J. Thompson, and A. Zervos, "The influence of soil nonlinear properties on the track/ground vibration induced by trains running on soft ground," *Transp. Geotech.*, vol. 11, pp. 1–16, 2017.

- [39] P. Thach, H. Liu, and G. Kong, "Vibration analysis of pile-supported embankments under high-speed train passage," *Soil Dyn. Earthq. Eng.*, vol. 55, pp. 92–99, 2013.
- [40] M. Banimahd, P. Woodward, J. Kennedy, and G. Medero, "Three-dimensional modelling of high speed ballasted railway tracks," *Proc. Inst. Civ. Eng. - Transp.*, vol. 166, no. 2, pp. 113–123, 2013.
- [41] M. J. M. M. Steenbergen and A. V. Metrikine, "The effect of the interface conditions on the dynamic response of a beam on a half-space to a moving load," *Eur. J. Mech. A/Solids*, vol. 26, no. 1, pp. 33–54, 2007.
- [42] S. B. Mezher, D. P. Connolly, P. K. Woodward, O. Laghrouche, J. Pombo, and P. A. Costa, "Railway critical velocity - Analytical prediction and analysis," *Transp. Geotech.*, vol. 6, no. October, pp. 84–96, 2016.
- [43] N. Yoshida, S. Kobayashi, I. Suetomi, and K. Miura, "Equivalent linear method considering frequency dependent characteristics of stiffness and damping," *Soil Dyn. Earthq. Eng.*, vol. 22, pp. 205–222, 2002.
- [44] Y. . Chen, C. J. Wang, Y. P. Chen, and B. Zhu, "Characteristics of stresses and settlement of ground induced by train," in *Environmental vibrations: Prediction, monitoring, mitigation and evaluation: Proceedings of the International symposium on environmental Vibrations*, 2005, pp. 33–42.
- [45] I. Ishibashi and X. Zhang, "Unified dynamic shear moduli and damping ratio of sand and clay," *Soils Found*, vol. 33, no. 1, pp. 182–191, 1993.
- [46] P. Alves Costa, P. Lopes, and A. S. Cardoso, "Soil shakedown analysis of slab railway tracks : Numerical approach and parametric study," *Transp. Geotech.*, vol. 16, no. July, pp. 85–96, 2018.